ULTRA-LOW-VOLTAGE GYROSCOPES BASED ON PIEZORESISTIVE NEMS FOR DRIVE-MOTION AND CORIOLIS-MOTION SENSING

Stefano Dellea[1], Giorgio S. Strazzeri[1], Patrice Rey[2], and Giacomo Langfelder[1]
[1]Politecnico di Milano, Milano, ITALY
[2]Cea-LETI, Grenoble, France

ABSTRACT

The work presents first gyroscopes based on NEMS gauges used both for sense-motion detection and for drive-motion detection. In such a configuration, no structural element is biased at voltages larger than 1 V, so 1 to 2 orders of magnitude lower than the DC voltage conventionally applied to the rotor of capacitive gyroscopes. Following the mechanical design, also the electronics is adapted, here relying on resistive sensing also in the drive loop, which guarantees an optimal rejection of feedthrough issues.

Within an area of about 1.1 $(mm)^2$ per axis, with drive mode Q factors of about 35000 at 0.3 mbar, 1.4 dph/√Hz angle random walk (ARW) is obtained. Bias stability given by NEMS 1/f noise becomes well visible.

INTRODUCTION

State of the art for miniaturized low-power gyroscopes is represented by micromachined structures based on capacitive drive-actuation, capacitive drive-detection and capacitive detection of the amplitude-modulated (AM) displacement induced by the Coriolis force. Simultaneous repeatability from part to part, stability, bandwidth and power consumption requirements can be matched in open-loop sense mode readout and in a mode-split configuration [1-4]. Recently proposed alternative working principles for further improved stability, like frequency-modulated gyroscopes [5, 6], also rely on capacitive actuation and detection.

In all referenced works, capacitive sensing interfaces require large voltages applied at the rotor port, to minimize both electronic noise of the sense chain and phase noise in the drive loop [7]. This is inherently related to the fact that the signal at the output of a varying capacitor biased with a DC value increases with the applied voltage. Typical rotor values of 10-50 V lead to ARW of about 5-20 mdps/√Hz in commercial products.

Gyroscopes based on piezoresistive gauges with sub-micrometric cross-section (NEMS) for Coriolis-motion detection were recently proposed in [8, 9]: such structures show sub-mdps/√Hz performance in compact area [10], but still require large in-operation voltages, as the drive resonator is capacitively comb-driven and comb-sensed.

In general, high voltages demand charge pumps to rise the native battery value, resulting in extra power dissipation from associated circuitry. Furthermore, capacitive drive resonators can suffer from known feedthrough effects [11].

The use of piezoresistive NEMS gauges also as drive-detection elements, as proposed in this work, definitely lowers the required voltages. As the gauges are incorporated within the drive springs, this approach also eliminates the area taken up by the drive-detection combs. The newly developed electrical equivalent model for such a drive resonator shows how feedthrough effects are made substantially irrelevant. Theoretical predictions finally indicate, for the gyroscope sensitivity, an intrinsic rejection of possible sensitivity changes due to temperature effects afflicting the gauge factor.

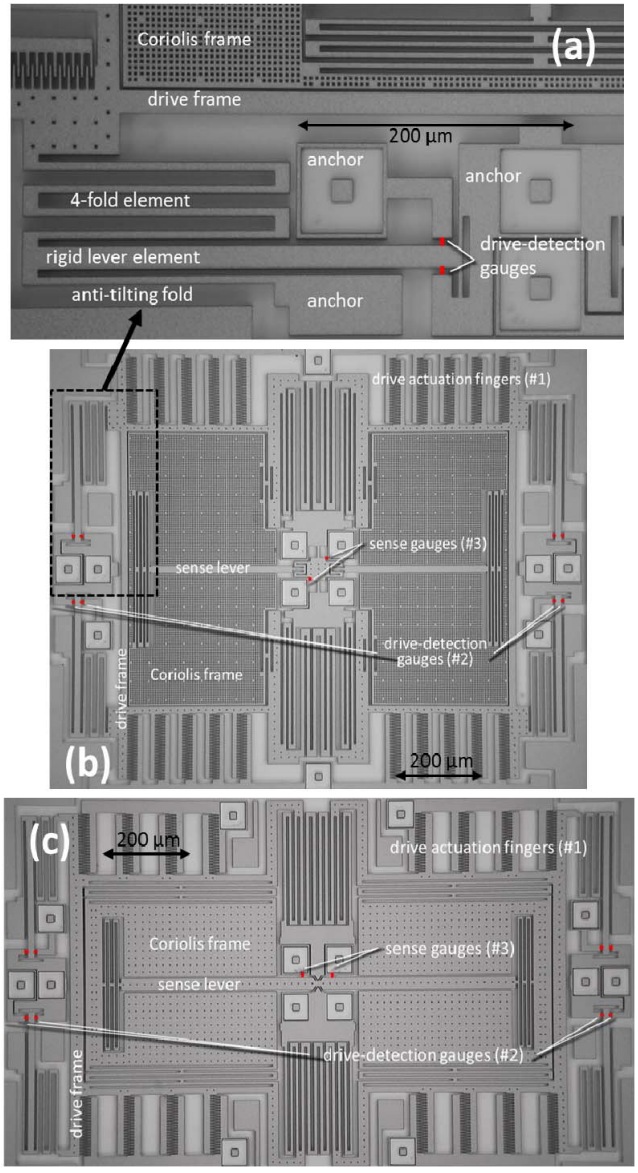

Figure 1: (a) top-view of the drive spring system formed by four folds and a lever, used to sense the drive motion with NEMS gauges. This configuration can be embedded in both Y-axis and Z-axis gyroscopes as shown in (b) and (c). For sake of clarity, the position of all 5-µm-long NEMS gauges is highlighted by red dashes (not to scale). The Z-axis sensor area is 780x1390 $(\mu m)^2$, the Y-axis sensor area is 950x1195 $(\mu m)^2$. Devices operate around 20 kHz with a mode-split value of about 500 Hz, packaged via Au-Si eutectic bonding at a 0.3 mbar pressure.

PROCESS AND DEVICES DESCRIPTION

The used M&NEMS process [8] from CEA-Leti enables the definition of (i) structural elements (frames, capacitors, springs), similarly to conventional surface micromachining processes [12], but at the same time of (ii), piezoresistive, monocrystalline Silicon beams with a sub-micrometric, (250 nm)^2, cross-section, defined and etched from the native Silicon-on-insulator (SOI) layer before the epitaxial growth. Their nominal resistance R_g is in the order of 2 kΩ for the designed 5 µm length; their nominal gauge factor *GF* (relative resistance change per unit axial strain) is in the order of 50.

Such NEMS gauges can be embedded as miniaturized sensing elements in a levered sense mode, as already described in previous works. However, while typical displacements of the sense mode can be as large as few 10s nm only, even under full-scale-range rates, the major design challenge in this work is the integration of NEMS elements also to sense the drive motion, whose displacement can be as large as 5 µm or more. The inclusion of the gauges in the drive mode, simultaneously respecting the drive frequency constraints and without exceeding the gauges maximum stress for linear piezoresistive response (about 0.5 to 1 GPa) requires therefore a specific design.

To this purpose, a dedicated type of drive spring is designed, formed by a rigid lever in series to flexible folds (Fig. 1a), such that the partitioned stress delivered to a pair of differential NEMS gauges, linked to the lever, is within their piezoresistive linearity limit. A further fold is designed on the opposite side of the lever as an anti-tilting element to shift spurious modes to high frequencies.

Figures 1b-c show a scanning-electron-microscope top view of the Y- and Z-axis gyroscopes, based on an in-plane drive mode that incorporates four of the described springs (one at each corner). Among the eight gauges involved, only four are used for drive-mode detection; the other four ones are dummy elements that guarantee mechanical symmetry. The gyroscopes are designed with a doubly-decoupled architecture with (#1) comb-based, electrostatically-excited and (#2) resistively-sensed drive mode (as described), and with (#3) resistively-sensed Coriolis mode. A single central lever is used in both devices to couple the two sense frames to the Coriolis frames for out-of-plane and in-plane rotational sense motion, respectively. Overall, 10 NEMS are thus designed in each device (and thus 30 for a 3-axis gyroscope). Note again the absence of the comb fingers for drive detection.

With the aid of finite-element simulation tools, the drive-mode frequency is nominally set to 21 kHz and 19 kHz for the Y- and Z-axis devices (such a frequency separation aims at minimizing cross-couplings), with the sense-mode frequency nominally split by 500 Hz, above the corresponding drive mode. The epitaxial process height of the structural layer is nominally h = 20 µm.

Packaging occurs via Au-Si eutectic bonding, which provides both the hermetic sealing and the electrical contacts between the MEMS and all interconnections. The latter are designed with two metal layers on the cap wafer. Getter is also patterned on the cap wafer, to lower the final package pressure to about 0.3 mbar.

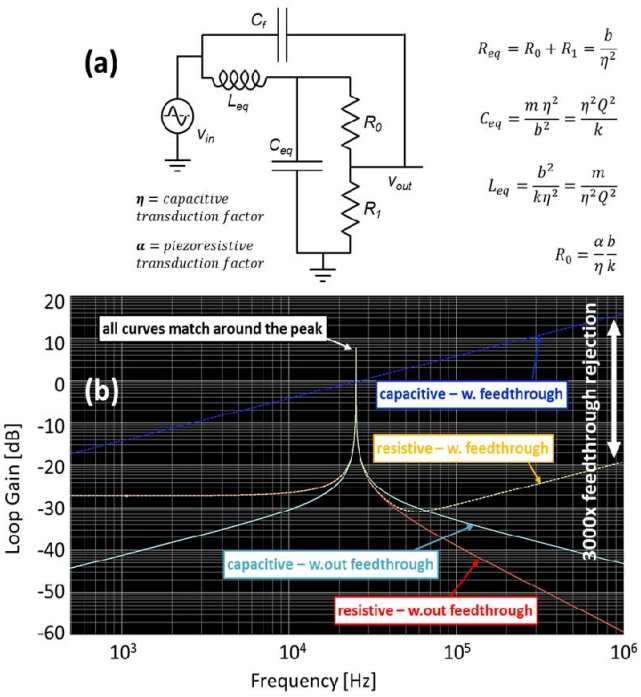

Figure 2: electrical equivalent model of the proposed resistively sensed resonator (a). Its open-loop transfer function inside the circuit is plotted in presence and absence of feedthrough effects, and compared to a capacitive resonator (b) normalized to the same peak amplitude, showing more than 3 orders of magnitude larger feedthrough rejection.

ELECTRICAL EQUIVALENT MODEL

The so-designed drive resonators have the electrical equivalent model shown in Fig. 2a, between the drive AC actuation voltage v_{in} and the drive-motion sensed voltage v_{out}, measured at the output of the NEMS gauges used in a differential Wheatstone bridge configuration. Fig. 2b plots the v_{out}/v_{in} transfer function (which has the same shape of an open-loop gain, neglecting electronic singularities). The absence of the zero in the origin (usually given by the capacitive sensing) makes the overall resonator loop-gain decrease by -40 dB/decade after resonance (red curve).

For comparative purposes, the model of a comb-driven and comb-sensed identical resonator is reported in light-blue (normalized to the same peak value), showing the initial +20 dB/decade growth and the -20 dB/decade decrease after resonance.

If now effects of direct, undesired, capacitive couplings between the drive and the sense ports are taken into account (dashed curves), one can notice the much better (more than three orders of magnitude) feedthrough rejection of the proposed resistively sensed resonator.

EXPERIMENTAL RESULTS

The devices are operated with the circuit of Fig. 3, which includes a differential Wheatstone-bridge as the front-end interface for both the modes. As shown in the inset, the presence of a secondary loop in the drive mode makes the overall sensitivity self-independent both on Q-factor and on gauge-factor variations, either from part to part, or with temperature or supply.

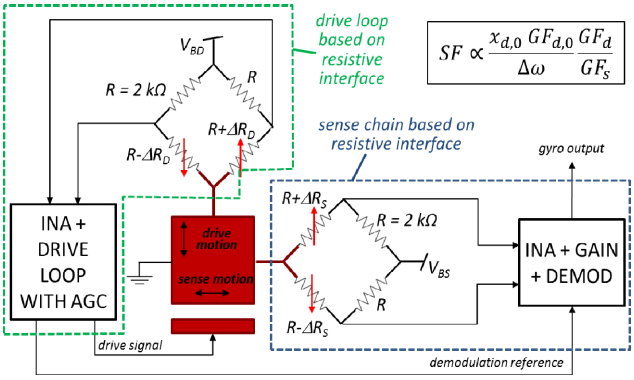

Figure 3: block-scheme of the electronics to control and sense the proposed gyroscopes. The circuit is based on resistive readout for both the drive- and sense-motion front-ends. The gain-control (AGC) in the drive loop reacts on the product of the drive amplitude $x_{d,0}$ times the nominal NEMS gauge factor $GF_{d,0}$, thus keeping the sensitivity SF proportional to a gauge-factor ratio, and thus independent of gauge-factor changes given by temperature variations.

The electronics is implemented with discrete components on a printed circuit board (PCB) which hosts a ceramic carrier where the MEMS gyroscopes are glues and wire-bonded. The PCB is mounted on an *Acutronic* rate table (AC1120-S). The suspended proof mass is kept to the ground potential; bridges DC supplies bias one end of all gauges to 0.2 V; drive combs are biased with a DC voltage of 1 V and a much smaller AC voltage. All structural elements of the sensor are thus biased at voltages compatible with typical integrated circuit supply.

Under an actuation ramp sweeping the rate between ±500 dps, the Z-axis device scale-factor responses shown in Fig. 4 are obtained at different drive amplitudes in the range 2.6 µm to 5.0 µm (the response of the Y-axis sensor at the maximum displacement is also reported). Note how the scale-factor deviation from the best linear fitting is characterized by few-ppm linearity errors, even at the largest drive motion amplitude, as shown in Fig. 5.

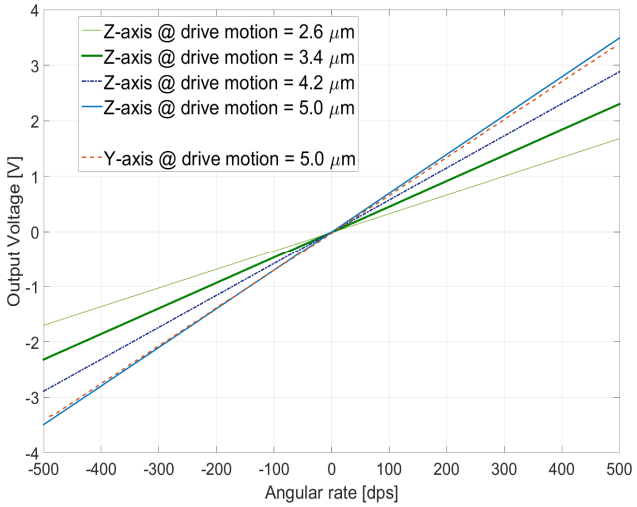

Figure 4: Z- and Y-axis gyroscope output response under a rate ramp, captured at different nano-gauge-detected drive-motion amplitudes. The gauge bias current is 40 µA.

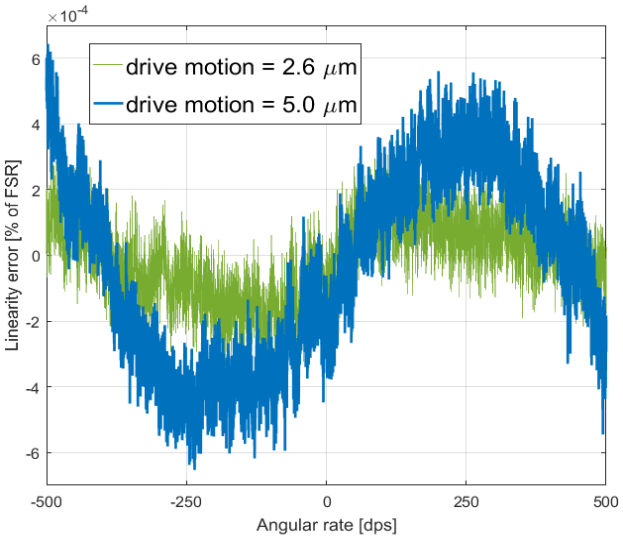

Figure 5: Z-axis device scale-factor linearity errors: values lower than 2 ppm and 6 ppm of the FSR are obtained for the minimum and the maximum drive amplitudes used in Fig. 4.

The input-referred quadrature values of 200 dps (Z-axis) and 5000 dps (Y-axis, likely due to skew angle issues), measured on average over 15 samples per type, are in line with typical gyroscope values, indicating that the used drive spring system does not significantly affect this parameter.

Fig. 6 finally reports measured noise performance (Z-axis device only) through the root Allan variance graph in uncontrolled laboratory environment: one can note a 400 µdps/√Hz (1.4 dph/√Hz) angle random walk at low observation intervals, after which a clear 1/f plateau is visible, likely generated by the gauge 1/f noise component. Finally, a rate random walk of 0.7 dph·√Hz becomes visible, setting the stability time at about 20 s.

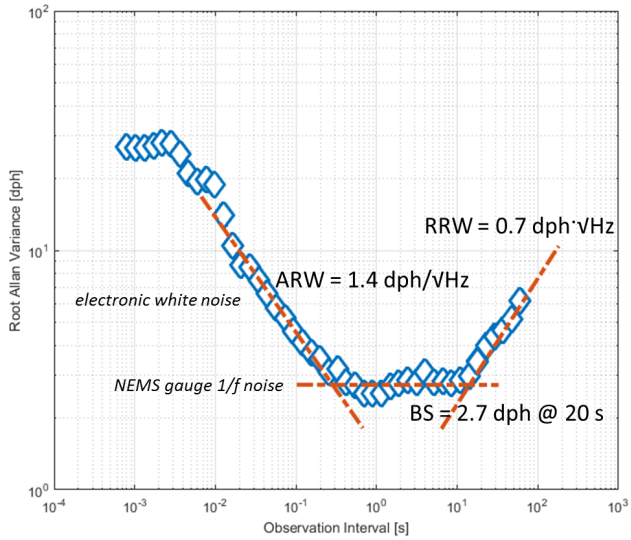

Figure 6: root Allan variance curve captured for the Z-axis gyroscope at a drive motion amplitude of 5 µm. Angle random walk is < 1.4 dph/√Hz. Stability given by the 1/f noise of the NEMS gauges is visible. Instability can be observed at 10 s of observation interval corresponding to a rate random walk of 0.7 dph·√Hz only.

Future works will include the experimental verification of the scale factor stability under temperature changes, as well as a reliability campaign to shock and drop tests, following the procedure presented in [13].

The work opens new chances for all those application areas where ultra-low-voltage, low-power miniaturized gyroscopes are demanded, in particular the field of implantable medical devices for restoration of vestibular functionalities.

ACKNOWLEDGEMENTS

The work was supported by the European Union under the FP7-ICT program "Nine-axis inertial sensors based on piezoresistive nano-gauge Detection" (NIRVANA) under grant agreement n. 288318. Part of the experiments was conducted in the MEMS&3D lab facilities of Politecnico di Milano.

REFERENCES

[1] V. Kempe, "Gyroscopes," in Inertial MEMS: Principles And Practice. Cambridge, U.K.: Cambridge Univ. Press, 2011, ch. 8.

[2] L. Prandi et al., "A low-power 3-axis digital-output MEMS gyroscope with single drive and multiplexed angular rate readout," in Proc. IEEE Int. Solid-State Circuit Conf. (ISSCC), San Francisco, CA, USA, Feb. 2011, pp. 104–106.

[3] G. Langfelder, S. Dellea, A. Berthelot, P. Rey, A. Tocchio, and A. F. Longoni, "Analysis of mode-split operation in MEMS based on piezoresistive nanogauges," J. Microelectromech. Syst., vol. 24, no. 1, pp. 174–181, Feb. 2015.

[4] J.-T. Liewald, B. Kuhlmann, T. Balslink, M. Trachtler, M. Dienger, and Y. Manoli, "100 kHz MEMS vibratory gyroscope," J. Microelectromech. Syst., vol. 22, no. 5, pp. 1115–1125, Oct. 2013.

[5] S.A. Zotov, A.A. Trusov, A.M. Shkel, "High-Range Angular Rate Sensor Based on Mechanical Frequency Modulation," Journ. Microelectromech. Syst., 2012, vol. 21, no. 2, pp. 398-405.

[6] M. H. Kline et al., "Quadrature FM gyroscope," in Proc. IEEE 26th Int. Conf. MEMS, Taipei, Taiwan, Jan. 2013, pp. 604–608.

[7] B. Razavi, "A Study of Phase Noise in CMOS Oscillators," IEEE Journal Of Solid-State Circuits, Vol. 31, N. 3, March 1996, pp. 331-343.

[8] S. Dellea, F. Giacci, A. F. Longoni, G. Langfelder, "In-Plane and Out-of-Plane MEMS Gyroscopes Based on Piezoresistive NEMS Detection," Journal of Microelectromechanical Systems, Vol. 24, No. 6, pp. 1817-1826, December 2015.

[9] F. Giacci, S. Dellea, A. F. Longoni, G. Langfelder, "Vibrations Rejection in Gyroscopes Based On Piezoresistive Nanogauges", in Conference on Solid-State Sensors, Actuators and Microsystems (Transducers 2015), pp. 780-783, June 2015.

[10] S. Dellea, F. Giacci, A. F. Longoni, P. Rey, P. Robert, G. Langfelder, "Analysis of Gyrocompassing through Miniaturized MEMS Based on Piezoresistive Sensing," proc. IEEE Inertial Sensors 2016, Laguna Beach (CA), February 2016.

[11] G. Langfelder, A. Caspani, and A. Tocchio, "Design criteria of low-power oscillators for consumer-grade MEMS resonant sensors," IEEE Transactions on Industrial Electronics, vol. 61, no. 1, pp. 567–574, Jan. 2014.

[12] G. Langfelder, S. Dellea, F. Zaraga, D. Cucchi, and M. A. Urquia, "The dependence of fatigue in microelectromechanical systems from the environment and the industrial packaging," IEEE Transactions on Industrial Electronics, vol. 59, no. 12, pp. 4938–4948, Dec. 2012.

[13] S. Dellea, F. Giacci, A. Capodici, P. Rey, G. Langfelder, "Reliability of gyroscopes based on piezoresistive nano-gauges against shock and free-drop tests," proc. MEMS 2016, Shanghai, CHINA, 24-28 January 2016, pp. 255-258.

CONTACT

*S. Dellea, tel:+39-0223996152; stefano.dellea@polimi.it